Room-Temperature Epitaxial Growth of Zn-Doped Iron Oxide Films on c-, a-, and r-Cut Sapphire Substrates

Valérie Demange, Xavier Portier, Sophie Ollivier, Mathieu Pasturel, Thierry Roisnel, Maryline Guilloux-Viry, Christian Hebert, Magdalena Nistor, Christophe Cachoncinlle, Eric Millon, et al.

Room temperature epitaxial growth of Zn-doped iron oxide films on c-, a- and r-cut sapphire substrates

Journal:	*Crystal Growth & Design*
Manuscript ID	cg-2023-004046.R3
Manuscript Type:	Article
Date Submitted by the Author:	n/a
Complete List of Authors:	Demange, Valérie; Université de Rennes, Institut des Sciences Chimiques de Rennes Portier, Xavier; Université de Caen Normandie, Centre de recherche sur les Ions, les MAtériaux et la Photonique (CIMAP), CEA/UMR CNRS 6252 Ollivier, Sophie; Université de Rennes, Institut des Sciences Chimiques de Rennes Pasturel, Mathieu; Université de Rennes, Institut des Sciences Chimiques de Rennes, UMR CNRS 6226 Roisnel, Thierry; Université de Rennes, Institut des Sciences Chimiques de Rennes Guilloux-Viry, Maryline; ISCR Hebert, Christian; Sorbonne Université, Institut des NanoSciences de Paris (INSP), CNRS UMR 7588 NISTOR, Magdalena; National Institute for Laser Plasma and Radiation Physics, Plasma Physics and Nuclear Fusion Laboratory (L22) Cachoncinlle, Christophe; Université d'Orléans, GREMI UMR 7344 Millon, Eric; Université d'Orléans, GREMI UMR 7344 Perrière, Jacques; Sorbonne Université, Institut des NanoSciences de Paris (INSP), CNRS UMR 7588

Room temperature epitaxial growth of Zn-doped iron oxide films on c-, a- and r-cut sapphire substrates

Valérie Demange[1,], Xavier Portier[2], Sophie Ollivier[1], Mathieu Pasturel[1], Thierry Roisnel[1], Maryline Guilloux-Viry[1], Christian Hebert[3], Magdalena Nistor[4], Christophe Cachoncinlle[5], Eric Millon[5], Jacques Perriere[3]*

[1] Univ Rennes, CNRS, ISCR – UMR 6226, ScanMAT – UAR 2025, F-35000 Rennes, France

[2] Centre de recherche sur les Ions, les MAtériaux et la Photonique (CIMAP), CEA/UMR CNRS 6252, Normandie Université, ENSICAEN, 14050 Caen Cedex, France

[3] Institut des NanoSciences de Paris (INSP), CNRS UMR 7588 Sorbonne Université, 4 Place Jussieu, Paris Cedex 05 75252, France

[4] National Institute for Lasers, Plasma and Radiation Physics (NILPRP), PO Box MG-36, 077125 Magurele-Bucharest, Romania

[5] GREMI UMR 7344 CNRS-Université d'Orléans, 45067 Orléans Cedex 2, France

KEYWORDS: Oxide thin film. Room-temperature epitaxy. Van der Waals Epitaxy. Graphoepitaxy. Pulsed laser deposition.

ABSTRACT. The room temperature growth of zinc-doped iron oxide films ($Zn:FeO_{x)}$) was studied on c-cut, a-cut and r-cut sapphire substrates using the pulsed-laser deposition method. Rutherford backscattering spectrometry, X-ray diffraction analysis, pole figure measurements and transmission electron microscopy were used to determine the nature of the oxide phases (wüstite and/or spinel) present in the films, their precise texture and in-plane epitaxial relationships between films and substrates. On c-cut sapphire, both wüstite and spinel phases were present with a (111) texture. The wüstite phase was mainly found at the film-substrate interface, while the spinel was observed in the upper part of the film. On the a-cut and r-cut substrates, the main phase observed was the wüstite, with a very small spinel contribution. The (111) and (100) wüstite textures were obtained on the a-cut and r-cut substrates, respectively. The in-plane epitaxial relationships between the Zn doped iron oxide phases and the substrates were deduced from transmission electron spectroscopy observations and pole figure measurements. The possible mechanisms of the room temperature epitaxial growth of the oxide films on r-cut and a-cut sapphire substrates are presented and discussed.

Introduction

As it has been largely demonstrated in literature, the epitaxy of oxide thin films on single crystalline substrates usually requires high temperature during the growth [1–5]. However, for a lot of industrial applications based on such epitaxial films, it would be necessary to reduce the growth temperature to avoid atomic interdiffusion between film and substrate, and consequently to significantly reduce the fabrication cost [6]. In this framework, research activities have been carried out to study room temperature (RT) epitaxial growth of oxide films like NiO [7,8], Fe_3O_4 [9], V_2O_3 [10], CoO and Co_3O_4 [11], and other oxides [12–14]. In most of these works, the RT epitaxial oxide films

were grown on atomically stepped single crystal sapphire (00l) substrates by using the pulsed-laser deposition (PLD) method [7–14]. Such stepped c-cut sapphire substrates are obtained by a thermal annealing process at high T (1000°C) for a few hours in air [15,16]. The surface steps play the role of nucleation centers for the epitaxial growth of the film. On the other hand, PLD is used for the film growth at RT owing to one of the specificities of this method, i.e. the high kinetic energy of the species emitted by the target during laser irradiation. Indeed, such a high kinetic energy (about a few 10th eV) [17] allows a high surface mobility for the species that leads to the formation of crystalline material at relatively low temperature [18,19].

In addition to the RT epitaxial growth of oxide films on c-cut (00l oriented) sapphire substrates, some other papers report the RT epitaxy of oxide films on single crystal substrates like MgO [20], $SrTiO_3$ [21], bare Si [22–24] or Si covered by a buffer layer [25]. However, some other single crystal substrates like a-cut ((110) oriented) and r-cut ((102) oriented) sapphire substrates are currently used for the epitaxial growth of various oxide films [26–31] with a view of specific applications [32–34]. To our knowledge, the RT epitaxy of oxide films on such a-cut and r-cut sapphire substrates has never been reported.

In this frame, we have studied the growth by PLD at RT of Zn-doped iron oxide on a-cut and r-cut sapphire substrates. For comparison purpose, ZFO films were also grown on a c-cut substrate, but more complex results obtained with this substrate will be published later in a forthcoming paper. Owing to the experimental PLD conditions used, two iron oxide-based phases are obtained: the Zn-doped wüstite phase Zn:FeO that will be noted "ZFO_w" in the following and the Zn-doped Zn:Fe_3O_4 spinel magnetite phase (noted "ZFO_s"). More precisely, $Zn_{1-x}Fe_xO$ films with ($0 < x < 1$) can be grown by PLD: following previous work[35], the Zn:Fe_3O_4 phase is obtained for $0.65<x<1$. We have chosen a Zn concentration fixed at around 25% at. ($x = 0.75$) to avoid the

formation of the wurtzite phase. In addition, the presence of Zn in the iron oxide phases should promote the growth the wustite phase even at low temperature (T < 500°C) as evidenced by Sano et al. [36]. We present here a detailed structural study of these phases deposited at RT on the various sapphire substrates: growth, textures and epitaxial relationships between these compounds and the different substrates are discussed. Such films could be of interest due to their magnetic properties since wüstite-based films are expected to be antiferromagnetic while magnetite-based films should be ferrimagnetic. These properties would permit the development of magnetite-based storage or spintronics devices [37,38], while wüstite could be used as a transparent p-type conductors [39] or for magnetoresistance enhancement [40]. However, these interesting physical properties are not the subject of this paper which is devoted to the detailed study of the structural properties of these films.

In our work, in contrary to the common high T annealing of the substrates before the film growth, all the c-, a- and r-cut sapphire substrates were not submitted to a thermal treatment at high T before the growth. Despite this point, we obtained the epitaxial growth at RT of the Zn-doped wüstite (ZFO_w, space group *Fm*-3*m*) and/or spinel (ZFO_s, *Fd*-3*m*) phases in the films. Different textures were obtained for these phases on the following type of substrates, i.e. (111) for the c-cut and a-cut sapphire, and (00l) for the r-cut one. Well-defined epitaxial relationships were found between films and substrates, and they have been described in the frame of the "domain matching epitaxy" (DME) [41–44]. The different textures observed depending on the substrates, could be explained either by (i) the graphoepitaxy related to the presence of steps and terraces on the c-cut and a-cut substrates[44-46], (ii) a "quasi van der Waals epitaxy" related to the polar nature of the c-cut and a-cut substrate plane and/or film plane [47–50], and (iii) an epitaxy related to a low lattice mismatch between the film and substrate in the case of the r-cut sapphire substrate.

Experimental section

The Zn-doped iron oxide films were grown by PLD onto c-cut, a-cut and r-cut sapphire substrates at RT in vacuum. The substrates furnished by CrysTec GmbH were not annealed at high T before the growth. A frequency quadrupled Nd-doped yttrium aluminum garnet (Nd:YAG) laser (266 nm, τ = 7 ns) was used to ablate a Zn:Fe_3O_4 ($Zn_{0.85}Fe_{2.15}O_4$) target in the experimental set up already described elsewhere [51]. The PLD growth from a Zn:Fe_3O_4 target can lead to the formation of nanocomposite films [52,53], i.e. with the presence of the wüstite (Zn:FeO) and spinel (Zn:Fe_3O_4). In contrary to the spinel phase, which has been epitaxially grown at RT [9], the wüstite phase has never been obtained in these conditions. In our work, we have tried to favor the growth conditions for the epitaxy of the wustite phase at RT. Indeed, the difference in oxygen composition between the wüstite, [O]/[Fe] = 1.1, and the spinel, [O]/[Fe] =1.33, means that the film must be grown under a low oxygen pressure. PLD allows oxygen incorporation in the oxide films to be controlled [54–58]. On one hand, the films on a-cut and r-cut substrates were thus grown under reducing conditions (residual vacuum: 2 10^{-7} mbar), i.e. a priori the ideal conditions for the formation of the wustite phase. On the other hand, the ZFO film on c-cut substrate was grown at 7 10^{-6} mbar leading to the presence of both wüstite and spinel phase.

Atomic force microscopy (AFM) was used to study the surface topography of the bare substrates before the growth, using an AFM NT-MDT Ntegra instrument.

Rutherford backscattering spectrometry (RBS) using the 2.5 MeV ion accelerator (SAFIR) of the Sorbonne Université, allowed the film thickness and in-depth distribution of the elements to be determined. The spectra, not presented here, show that the Zn-doped iron oxide films are only constituted by Fe, Zn and O atoms, without the presence of any impurities. The precise

concentration profile of the Zn, Fe and O elements has been obtained from the simulation of the RBS spectra by use of the RUMP simulation program and has allowed to deduce the [O]/[Fe] ratio in the films.

X-ray diffraction (XRD) has been performed on a Bruker D8 Advance θ-2θ diffractometer in modified Bragg-Brentano geometry, working with monochromatized Cu Kα1 radiation (λ = 1.5406 Å) and equipped with a LynxEye detector. The sample was rotated at a speed of 30 rpm during measurement. Le Bail profile refinement using the Fullprof software [59] of the XRD patterns of ZFO films grown on a-cut and r-cut sapphires enabled to precise unambiguously whether ZFO_w and ZFO_s phases are both present and to estimate the cell parameters of these phases. For these refinements, the "zero"-shifts due to the sample positioning were first determined from the 2θ-shifts of the substrate Bragg peaks, and then fixed to enable the refinement of the cell parameters of the iron oxide phases. The texture of the films and the in-plane relationships with the substrate were investigated by pole figure measurements with the help of a Bruker D8 Discover diffractometer (Cu Kα1,2 radiation).

For transmission electron microscopy (TEM) observations, thin foils were thinned down to electron transparency by a focused ion beam (FIB) setup (Dual-beam FEI Helios nanolab 660) with an electron imaging resolution of 0.6 nm at 15 kV (Field emission gun (FEG)) and a FIB resolution of 2.54 nm at 30 kV. TEM experiments were performed using a double corrected cold FEG JEOL ARM 200F microscope, operated at 200 kV and equipped with a post column GATAN QUANTUM ER electron energy loss spectrometer (EELS). This microscope had also a scanning setup (STEM mode with dark and bright field detectors) allowing the electron beam to be monitored with a spatial resolution of about 0.078 nm. Altogether, STEM EELS experiments were

then possible in order to obtain EELS spectra for a nanometer region, EELS profiles or even EELS mapping. All digitized images and spectral data were processed using the commercial Digitalmicrograph (GMS2) software from GATAN.

Results

Before the RT growth of ZFO films on the single crystal substrates, AFM images of the surface of these substrates were registered. Figure 1 shows the surface morphology of the c-cut (Fig. 1(a)), a-cut (Fig. 1(b)) and r-cut (Fig. 1(c)) sapphire substrates as furnished by CrysTec GmbH.

Both c-cut and a-cut sapphire substrates show not very well defined and very narrow steps without terraces, while the surface of the r-cut sapphire does not show any steps or terraces but only a few spikes. This work mainly aimed at checking the possible RT epitaxy of ZFO films on a- and r-cut sapphire substrates. First, we have looked at the possible RT epitaxy of ZFO on a c-cut substrate. Indeed, the RT epitaxy of Zn (25%at.) doped Fe_3O_4 has not been previously reported on c-cut substrate. Therefore, the PLD growth of such a film on a c-cut substrate at RT under a $7x10^{-6}$ mbar oxygen pressure has been studied. Figure 2 reports the corresponding XRD pattern of such film and shows first, a broad peak at about 18° related to the (111) spinel phase with refined cell parameter $a_s = 0.8529 \pm 0.0005$ nm, i.e. higher than the expected theoretical value for undoped Fe_3O_4 ($a = 0.83905$ nm, *Fd*-3*m*). Secondly, a broad asymmetric peak around 36° corresponding to the superimposition of 222 spinel and the 111 wüstite Bragg reflections is observed. Despite the low intensity of the 111 ZFO_w peak, the cell parameter is around $a_w = 0.43217 \pm 0.0005$ nm, a value slightly higher than for the undoped FeO phase ($a = 0.4307$ nm, *Fm*-3*m*) (Table 1).

Table 1. Composition determined by RBS and crystallographic features determined by XRD of ZFO films grown at RT on c-cut, a-cut and r-cut sapphires (W: wüstite, S: spinel). The values of [O]/[Fe] does not consider oxygen bound to zinc and are only related to oxygen associated to iron.

Substrate	Composition	[O]/[Fe]	a_W	a_S	Preferential orientation	FWHM RC
c-cut	$Zn_{0.24}Fe_{0.76}O_{1.15}$ $(Zn_{0.24}O_{0.24})(Fe_{0.76}O_{0.91})$	1.19	0.43217 ± 0.005 nm	0.85289± 0.005 nm	(111) W (111) S	~ 1.8°
a-cut	$Zn_{0.23}Fe_{0.77}O_{1.12}$ $(Zn_{0.23}O_{0.23})(Fe_{0.77}O_{0.89})$	1.15	0.43435 ± 0.005 nm	-	(111) W	~ 1.9°
r-cut	$Zn_{0.23}Fe_{0.77}O_{1.1}$ $(Zn_{0.23}O_{0.23})(Fe_{0.77}O_{0.87})$	1.13	0.4317 ± 0.005 nm	0.8415 ± 0.005 nm	(100) W (100) S	4.7°

TEM analysis was led to precisely investigate the epitaxial growth of the ZFO film on c-cut sapphire substrate. Figure 3(a) shows a typical high resolution electron microscopy (HREM) image of a cross section of the film. The orientation of the sample is such that the electron beam is parallel to the [210] direction of Al_2O_3 sapphire (visible at the bottom of the image) and thus parallel to the film/substrate interface. In the upper region of the film, one can notice distinctly that we are dealing with a columnar growth with column widths of a few tens of nanometers whereas the bottom of the film appears more "uniform" without visible boundaries over a thickness of about 15 nm by contrast with the upper region.

By extracting and enlarging smaller regions from these parts of the film (shown in Fig. 3(b) for the rough images and 3(c) for the corresponding filtered images), an analysis of the lattice

fringes through Fast Fourier Transforms (FFTs) allows establishing the structural characteristics and then the corresponding phases. The FFTs presented in Fig. 3(d) reveal that the bottom part of the film is consistent with a face centered cubic structure along a [-101] direction with a lattice parameter of 0.43 nm. This agrees with the wüstite phase (FeO) doped with Zn (confirmed by chemical analyses, not shown). The corresponding orientation relationships between sapphire and ZFO_w are the following:

$$(111)\ ZFO_w\ //\ (003)\ Al_2O_3$$

$$[-101]\ ZFO_w\ //\ [210]\ Al_2O_3$$

As far as the upper region is concerned, the FFT of the enlarged image shows also a face centered cubic structure but with a lattice parameter close to that of the spinel phase Fe_3O_4. Zn is also present in the chemical composition of the compound and the orientation relationships between wüstite and magnetite are:

$$(111)\ ZFO_w\ //\ (111)\ ZFO_s$$

$$[-101]\ ZFO_w\ //\ [10\text{-}1]\ ZFO_s$$

To confirm the presence of both phases, a spectroscopic analysis using EELS method has been used. In Fig. 3(a), two spots are indicating the two pointed regions from which one obtained the EELS spectra presented in Fig. 4.

These spectra correspond to the L_2 and L_3 thresholds of Fe whose positions are indicative of the valence sate of Fe. A 1 eV displacement of the L_3 peak towards lower energies for the bottom of the film is clearly meaning a decrease in the valence state of Fe and then consistent with the

presence of the wüstite phase at the bottom of the film. Similar shift for these compounds has been reported in previous works [60]. The presence of the wüstite phase is also in agreement with the [O]/[Fe] ratio deduced from RBS measurements, the obtained values being between 1.13 and 1.19 (Table 1).

The XRD *θ-2θ* patterns recorded on the ZFO films grown on the a- and r-cut substrates are presented in Fig. 5. The data regarding the lattice parameters and the full width at half maximum (FWHM) of the rocking curves are summarized in Table 1. The XRD pattern (Fig. 5(a)) recorded for the film grown on the a-cut sapphire shows the presence of the 111 wüstite reflection at about $2\theta = 35.75°$. The 111 and 222 spinel peaks which would appear at 18° and 36.6° respectively, are not observed in this pattern. Profile refinement using a single FeO phase leads to satisfying modelisation of the observed peak and suggests that the film is constituted of a pure wüstite phase.

In Fig. 5(b), the XRD pattern corresponding to the film grown on the r-cut substrate shows a wide peak at about 41.75°. Best profile refinement is obtained by considering simultaneous presence of 200 and 400 Bragg reflections of ZFO_w and ZFO_s phases, respectively, showing a significant texture of these films. Due to the limited number of observed diffraction peaks, it is not possible to retrieve the proportional distribution of each phase from the refinement.

For the ZFO films grown on the a-cut substrate, the rocking curve (not shown here) of the respective 111 reflection peaks is rather narrow, i.e. 1.9°, taking into account the RT growth. On the contrary, for the ZFO film grown on the r-cut substrate, the value of the rocking curve of the 002 ZFO_w reflection was much more important, i.e. 4.7°. In this latter case, the crystalline quality of the film is poorer. It must be noticed that in the case of the epitaxial growth of various oxide films on r-cut sapphire substrate, the surface plane of the oxide film was tilted with respect to the

(102) plane of sapphire. This phenomenon was observed for instance in the epitaxial growth of ZnO [61], CeO_2 [62], MgO [63,64] or Fe_3O_4 [65]. The tilt can be important, for example the (100) MgO may epitaxially grow on (102) Al_2O_3 with a tilt up to 5 or 6°, depending upon the growth temperature. From such results, it was concluded that the surface state of r-plane sapphire is an important factor leading to the tilted growth of the epilayer [63-65]. In our present case, it is not surprising that the epitaxial growth of ZFO on r-plane Al_2O_3 occurs at RT with a tilt of about 4.7°.

Figure 6(a) shows the results of the epitaxial relationships study between the wüstite phase and the a-cut substrate. The phi-scan performed on the {200} planes of the ZFO_w phase (2θ = 42.391°; ψ = 56.22°) shows 6 peaks separated by 60°. In addition, phi-scan of the {104} planes of sapphire (2θ = 35.14°; ψ = 57.55°) was also performed to deduce the crystalline orientations of the film with respect to the substrate. It shows 2 peaks separated by 180° and located at about 6.2° of the closest peak of the film. Figure 6(b) shows the pole figure recorded with the 200 ZFO_w reflection (2θ = 42.39°) for the same film grown on the a-cut substrate. This figure presents 6 well defined poles at ψ equal to 56.22°, in agreement with the phi-scan in Fig. 6(a). Some other poles from the substrate are also observed at: i) ψ = 29° corresponding to the 113 Al_2O_3 reflection (owing to the angle between (110) and (113) planes (28.78°) and the Bragg reflection of (113) plane: 2θ = 43.36°) and ii) ψ = 64° corresponding to the -123 Al_2O_3 reflection (angle between (110) and (113) planes = 64.01° and 2θ (-123) = 43.36°).

From the azimuthal positions of the respective peak/poles of ZFO_w and Al_2O_3, it is demonstrated that the epitaxial relationships on the a-cut sapphire substrate correspond to the superposition of the hexagons of the (111) ZFO_w plane on the rectangular lattice of the a-cut

sapphire, with a slight disorientation between the two lattices, as shown in Fig. 7(a). Given this pattern, no match can be observed between the two lattices.

Actually, the explanation of the epitaxial growth of ZFO_w on Al_2O_3 is in the frame of the domain matching epitaxy (DME), with *m* lattice units of the film matching with *p* lattice units of the substrate [64], as shown in figure 7(b). This figure presents the in-plane lattices of ZFO_w and sapphire which are superimposed considering the 6.2° of rotation between the (2-20) plane of ZFO_W and the (1-1-4) plane of the sapphire. The interception of these planes with the in-plane lattices (traces) corresponds to the traces of the (200) plane of ZFO_W and the (10-4) plane of the sapphire chosen to carry out the phi-scans measurement. It can be seen in figure 7(b) that there is a coincidence of sites between the two lattices leading to a matching domain forming a parallelogram. Since the Bravais lattice of the sapphire is hexagonal, it is not possible to easily determine the directions which correspond to the sides of this parallelogram. We have therefore described the epitaxial relationships between the two lattices by instead considering rather the planes which form the parallelogram, as follows:

Out-of-plane: (111) ZFO_w // (110) Al_2O_3

In-plane (I) (11-2) ZFO_W // (1-12) Al_2O_3

In-plane (II) (-871) ZFO_W // (1-1-4) Al_2O_3

In-plane (III) (3-1-2) ZFO_W // (1-1-1) Al_2O_3

Only the shortest side of the parallelogram corresponds to a perfect fit of m lattice units (*m* = 5 for ZFO_W and *p* =1 for Al_2O_3). Therefore, lattice mismatches are determined by considering

the interatomic distances shown in figure 7(c). It appears that these distances are very close between the two lattices, corresponding to low mismatch values (cf. Table 2).

Table 2. Epitaxial relationships of Zn:FeO wüstite films grown at RT on a-cut and r-cut sapphires.

Substrate	**Epitaxial relationships**	**Domain matching relationships**		**Lattice mismatch δ (%)**	**Domain size D (nm)**
		m	***p***		
a-cut	(11-2) ZFO_W // (1-12) Al_2O_3	5	1	1.2	1.52
	(-871) ZFO_W // (1-1-4) Al_2O_3	-	-	-1.38	2.12
	(3-1-2) ZFO_W // (1-1-1) Al_2O_3	-	-	-2.21	2.78
r-cut	[100] ZFO_w // [010] Al_2O_3	11	10	-0.06	4.7
	[010] ZFO_w // [2-1-1] Al_2O_3	6	5	-1.28	2.6

Figure 8(a) displays the phi-scans of the ZFO film grown on r-cut sapphire recorded by selecting the {111} planes. It shows 4 peaks separated by 90° and located for the closest one at about 45.5° of the (006) substrate plane. The corresponding pole figure is shown in Fig. 8(b). Similarly, the pole figure (Fig. 8(b)) for the ZFO film grown on the r-plane Al_2O_3 was also recorded. From the azimuthal positions of the peaks/poles, the following epitaxial relationships were deduced:

$$(100)\ ZFO_w\ //\ (102)\ Al_2O_3$$

(I) $[100]\ ZFO_w\ //\ [010]\ Al_2O_3$

(II) $[010]\ ZFO_w\ //\ [2\text{-}1\text{-}1]\ Al_2O_3$

Such orientation relationships correspond to the superposition of the square lattice plane (001) of ZFO_w on the rectangular lattice of the (102) plane of Al_2O_3 substrate as shown in Fig. 9(a).

These two relationships lead in both case to rather large lattice mismatch, 9% for (I) and 15.6% for (II), respectively. Regarding the DME, as indicated in Table 2, a coincidence for relation (I) is obtained with 10 substrate units and 11 film units giving a -0.06% lattice mismatch. For the relation (II) the coincidence is realized with 5 substrate units and 6 film units with a -1.28% mismatch (Fig. 9(b)).

Discussion

In the previous works reported on the RT epitaxy of oxide films, results were usually obtained on c-cut sapphire substrates, and two main points play a role on this epitaxy. The first is the presence of steps and terraces on the c-cut surface. These steps and terraces are due to a miscut and / or a high T annealing of the c-cut sapphire substrate [15,16], which will play the role of nucleation centers for the epitaxial growth. This kind of growth corresponds to the graphoepitaxy [46]. The second point is the fact that the c-cut sapphire plane is polar, i.e. either a pure oxygen plane or a pure Al plane. In the case of the cubic oxides (NiO, Co_3O_4, Fe_3O_4, …), epitaxially grown at RT or at high T on c-cut substrate, the observed texture is (111), i.e. a plane which is also a polar plane [45]. The epitaxial growth concerns thus two polar planes, and this situation is very similar to the quasi van der Waals epitaxy [48,49] where there is only very little or no chemical bonding between the atoms of the film and substrate. Indeed, the stability and the epitaxy of the film-substrate interface are related to the weak electrostatic interaction between the two polar planes [50].

In the case of the ZFO epitaxial growth on c-cut substrate, the epitaxial relationships are the same as those observed in the case of the growth of ZFO on this substrate at elevated temperature [52], i.e. the growth occurs with a "30° rotation" of the hexagons of the (111) ZFO plane on the hexagon of the (002) sapphire plane**.** It should be reminded that, in this work, the substrate was not thermally treated, so the AFM image shows presence of steps, but however much less defined than the ones obtained with a high thermal treatment at 1000°C. Moreover, after the film growth, the AFM images (not shown) does not show any steps or terraces which is rather different from the results commonly reported in which steps and terraces are present at the surface of the oxide films grown at RT on c-cut substrates annealed at high temperature before the growth. In our case, polar nature of the c-cut sapphire substrate and of the (111) plane of the Zn-doped iron oxide may lead to an electrostatic interaction at this interface. Therefore, it seems reasonable to conclude that both the graphoepitaxy and the quasi van der Waals epitaxy are at the origin of the RT epitaxy of ZFO on c-cut sapphire substrate. Concerning the film grown on the a-cut substrate, it must be noticed that this substrate is also either a pure cationic or a pure oxygen one. Our results show that the RT epitaxy of the wüstite phase is based on the (111) ZFO_w plane, despite the fact that the a-cut substrate and the (111) ZFO_w present very different atomic configuration, i.e. a symmetry mismatch between the substrate (2-fold) and the (111) ZFO_w film (3-fold).

An interesting point which can be noticed is that such epitaxial relationship (111) ZFO_w // (110) Al_2O_3 corresponds to an epitaxy of a hexagon on a rectangle with different symmetries for these two planes. One can ask thus why an epitaxy with a square (ZFO_W) on a rectangle (r-cut Al_2O_3) is not observed while the square and rectangular configurations would be more relevant. Concerning the DME, it is possible to obtain the lattice mismatch δ and domain matching epitaxy

D in terms of the epitaxial relationships with (001) ZFO_w // (110) Al_2O_3. The calculated values of δ and D are the following:

[100] ZFO_w // [001] Al_2O_3 m = 3 p = 1 δ = 0.02 % D = 1.3 nm

[001] ZFO_w // [1-10] Al_2O_3 m = 19 p = 10 δ = 0.13 % D = 8.3 nm

The comparison of these values with those given in Table 2 for the (111) ZFO_w // (110) Al_2O_3 indicates that the epitaxy of the square (001) ZFO_w on the rectangular (110) Al_2O_3 is better in terms of DME. The reason why this epitaxy is not observed is certainly related to the fact that the (100) ZFO_w plane is not a polar plane, i.e. O and Fe are present in this plane. It can be concluded that the van der Waals epitaxy based on the electrostatic interaction between the (111) ZFO_w and the (110) Al_2O_3 is preferred to the simple "square on rectangular" epitaxy.

It follows thus that the (111) ZFO_w texture could be explained in the frame of an electrostatic interaction due to the "quasi Van der Waals epitaxy". Indeed, the (111) plane in the wüstite (FCC structure) is a polar plane, and the a-cut sapphire plane is also a polar plane. An electrostatic interaction between these two polar planes is thus envisaged in a similar way to the quasi van der Waals epitaxy.

For the ZFO film grown on the r-cut substrate, the (100) wüstite texture is observed. This is rather surprising since this situation is *a priori* similar to the a-cut substrate case. Indeed, the r-cut plane is either a pure oxygen plane or a pure cationic plane, and it presents a rectangular atomic configuration. As for the a-cut surface plane, the (111) wüstite texture could be expected, but the (100) wüstite texture is observed. This means that both the graphoepitaxy and/or van der Waals epitaxy cannot be envisaged to explain the epitaxial growth of ZFO on the r-cut sapphire substrate.

We mentioned above the specific problem of the tilt in the epitaxy on r-cut substrate, but another parameter is the growth temperature, which plays an important role in the epitaxial growth of oxide films on the r-cut substrate. For example in the case of CeO_2 films grown on a r-cut substrate thermally treated at high T (1000°C), steps and terraces are formed at the surface and a pure (100) CeO_2 texture is observed for example [28,67,68]. Moreover, the steps are formed along the [010] direction of the r-cut substrate, which is one of the in-plane directions of the epitaxy. On the contrary, when the r-cut substrate is not thermally treated at high temperature, steps and terraces are not formed, and both (111) and (100) CeO_2 textures are observed [28,67,68]. Further studies on CeO_2 films on r-cut substrates have shown that the growth temperature plays an important role on the film texture [69]. Indeed, the texture of CeO_2 films changed from (001) at 150°C to a mixed (001) and (111) textures at 300°C, and finally to pure (111) for increasing temperatures [4]. In our work, the presence of steps and terraces on the r-cut substrate (Fig. 1(c)) is not clearly evidenced from the AFM images, and furthermore only the (100) ZFO_w texture is observed. Moreover, our films are grown at RT, and we can thus assume that the (100) ZFO_w texture is due to the low growth temperature of the film in a similar way to the case of the CeO_2 film grown on r-cut sapphire substrates [69].

Conclusion

Using a Zn:FeO_x target, the wüstite (Zn:FeO) and/or spinel (Zn:Fe_3O_4) phases were obtained on c-cut, a-cut and r-cut sapphire single crystal substrates by pulsed laser deposition at room temperature. Depending upon substrates, the two textures, (111) or (100), may be obtained, and poles figures showed the RT epitaxy of the films on all substrates. The possible origin of these distinct textures and epitaxial relationships has been discussed according to both the « graphoepitaxy » and the « quasi van der Waals epitaxy » for the films grown on the c-cut and a-

cut substrates. For the film grown on the r-cut, the (100) texture is obtained as it has been observed in other cases. An important point in the RT epitaxy of the ZFO films is the high kinetic energy of the species emitted by the target during the laser ablation. Such a high kinetic energy of these species will give them the possibility to move on the substrate on sufficient long distances to find their site in the growth of the crystal structure. Finally, this work shows that the RT epitaxy of the oxide films is quite possible on various sapphire substrates (c-cut, a-cut and r-cut), and this opens the way to the PLD growth of oxide films on substrates like MgO, $MgAl_2O_4$ or others at RT.

AUTHOR INFORMATION

Corresponding Author

*Information for the author to whom correspondence should be addressed: Dr. Valerie Demange.

Valerie.demange@univ-rennes.fr

Author Contributions

The manuscript was written through contributions of all authors. All authors have given approval to the final version of the manuscript. VD performed the XRD characterizations and LeBail refinement, analyzed and interpreted the corresponding data and drafted the article. XP performed the TEM and EELS measurements, analyzed and interpreted the corresponding data and drafted the article. SO performed the AFM measurements. MP and TR performed LeBail refinement,

analyzed and interpreted the corresponding data. CH and MN synthetized PLD films, performed RBS measurements, analyzed and interpreted the corresponding data. MGV revised the manuscript. CC and EM analyzed and interpreted the data and drafted the article. JP conceived and designed the project, analyzed and interpreted the data and drafted the article.

Funding Sources

The research of the manuscript was supported by the French ANR (Agence Nationale de la Recherche) organisation and the Normandie Region in acquiring the EELS spectrometer and the FIB setup in the framework of the PAI program (ANR-11-EQPX-0020). XRD measurements were performed on Osirix platform (ScanMAT, UAR 2025 University of Rennes-CNRS), which received a financial support from the European Union through the European Regional Development Fund (ERDF), the Département d'Ille et Vilaine, Rennes Métropole and Région Bretagne (2015-2020 CPER project SCANMAT).

ACKNOWLEDGMENT

XP thanks Franck LEMARIE for his contribution in preparing the TEM samples. The agreement on cooperation between the National Institute for Lasers, Plasma and Radiation Physics (NILPRP) and the INSP, Université Pierre et Marie Curie –Paris 6 (now Sorbonne Université) is also acknowledged (M.N., J.P.).

ABBREVIATIONS

RT, room temperature; PLD, pulsed-laser deposition; ZFO_w, wüstite phase Zn:FeO; ZFO_s, Zn-doped Zn:Fe_3O_4 spinel magnetite phase; Nd:YAG, Nd-doped yttrium aluminum garnet; AFM, atomic force microscopy; RBS, Rutherford backscattering spectrometry; XRD, X-ray diffraction;

TEM, transmission electron microscopy; FIB, focused ion beam; FEG, Field emission gun; EELS, electron energy loss spectrometer; STEM, scanning transmission electron microscopy; HREM, high resolution electron microscopy; FFT, Fast Fourier Transform; FWHM, full width at half maximum; DME, domain matching epitaxy.

REFERENCES

(1) Chambers, S. A. Epitaxial Growth and Properties of Doped Transition Metal and Complex Oxide Films. *Adv. Mater.* **2010**, *22* (2), 219–248. https://doi.org/10.1002/adma.200901867.

(2) Narayan, J. Recent Progress in Thin Film Epitaxy across the Misfit Scale (2011 Acta Gold Medal Paper). *Acta Mater.* **2013**, *61* (8), 2703–2724. https://doi.org/10.1016/j.actamat.2012.09.070.

(3) Roemer, A.; Millon, E.; Vincent, B.; Boudrioua, A.; Pons-Y-Moll, O.; Defourneau, R. M.; Seiler, W. Epitaxial PbTiO3 Thin Films Grown on (100) MgO by Pulsed-Laser Deposition for Optical Waveguiding Properties. *J. Appl. Phys.* **2004**, *95* (6), 3041–3047. https://doi.org/10.1063/1.1649461.

(4) Nistor, M.; Seiler, W.; Hebert, C.; Matei, E.; Perrière, J. Effects of Substrate and Ambient Gas on Epitaxial Growth Indium Oxide Thin Films. *Appl. Surf. Sci.* **2014**, *307*, 455–460. https://doi.org/10.1016/j.apsusc.2014.04.056.

(5) Tricot, S.; Nistor, M.; Millon, E.; Boulmer-Leborgne, C.; Mandache, N. B.; Perrière, J.; Seiler, W. Epitaxial ZnO Thin Films Grown by Pulsed Electron Beam Deposition. *Surf. Sci.* **2010**, *604* (21), 2024–2030. https://doi.org/10.1016/j.susc.2010.08.016.

(6) Rasic, D.; Sachan, R.; Chisholm, M. F.; Prater, J.; Narayan, J. Room Temperature Growth of Epitaxial Titanium Nitride Films by Pulsed Laser Deposition. *Cryst. Growth Des.* **2017**, *17* (12), 6634–6640. https://doi.org/10.1021/acs.cgd.7b01278.

(7) Yamauchi, R.; Hamasaki, Y.; Shibuya, T.; Saito, A.; Tsuchimine, N.; Koyama, K.; Matsuda, A.; Yoshimoto, M. Layer Matching Epitaxy of NiO Thin Films on Atomically Stepped Sapphire (0001) Substrates. *Sci. Rep.* **2015**, *5* (1), 14385. https://doi.org/10.1038/srep14385.

(8) Kakehi, Y.; Nakao, S.; Satoh, K.; Kusaka, T. Room-Temperature Epitaxial Growth of NiO(111) Thin Films by Pulsed Laser Deposition. *J. Cryst. Growth* **2002**, *237–239*, 591–595. https://doi.org/10.1016/S0022-0248(01)01964-9.

(9) Liu, X.; Lu, H.; He, M.; Wang, L.; Shi, H.; Jin, K.; Wang, C.; Yang, G. Room-Temperature Layer-by-Layer Epitaxial Growth and Characteristics of Fe3O4 Ultrathin Films. *J. Phys. Appl. Phys.* **2014**, *47* (10), 105004. https://doi.org/10.1088/0022-3727/47/10/105004.

(10) Liu, X.; Lu, H.; He, M.; Jin, K.; Yang, G. Room-Temperature Epitaxial Growth of V2O3 Films. *Sci. China Phys. Mech. Astron.* **2014**, *57* (10), 1866–1869. https://doi.org/10.1007/s11433-014-5483-4.

(11) Matsuda, A.; Yamauchi, R.; Shiojiri, D.; Tan, G.; Kaneko, S.; Yoshimoto, M. Room-Temperature Selective Epitaxial Growth of CoO (111) and Co3O4 (111) Thin Films with Atomic Steps by Pulsed Laser Deposition. *Appl. Surf. Sci.* **2015**, *349*, 78–82. https://doi.org/10.1016/j.apsusc.2015.04.205.

(12) Takakazu Kiyomura, T. K.; Manabu Gomi, M. G. Room-Temperature Epitaxial Growth of Ni-Zn Ferrite Thin Films by Pulsed Laser Deposition in High Vacuum. *Jpn. J. Appl. Phys.* **1997**, *36* (8A), L1000. https://doi.org/10.1143/JJAP.36.L1000.

(13) Yoshimoto, M.; Yamauchi, R.; Shiojiri, D.; Tan, G.; Kaneko, S.; Matsuda, A. Room-Temperature Synthesis of Epitaxial Oxide Thin Films for Development of Unequilibrium Structure and Novel Electronic Functionalization. *J. Ceram. Soc. Jpn.* **2013**, *121* (1409), 1–9. https://doi.org/10.2109/jcersj2.121.1.

(14) Seo, O.; Tayal, A.; Kim, J.; Song, C.; Chen, Y.; Hiroi, S.; Katsuya, Y.; Ina, T.; Sakata, O.; Ikeya, Y.; Takano, S.; Matsuda, A.; Yoshimoto, M. Tuning of Structural, Optical Band Gap, and Electrical Properties of Room-Temperature-Grown Epitaxial Thin Films through the Fe2O3:NiO Ratio. *Sci. Rep.* **2019**, *9* (1), 4304. https://doi.org/10.1038/s41598-019-41049-9.

(15) Yoshimoto, M.; Maeda, T.; Ohnishi, T.; Koinuma, H.; Ishiyama, O.; Shinohara, M.; Kubo, M.; Miura, R.; Miyamoto, A. Atomic-Scale Formation of Ultrasmooth Surfaces on Sapphire Substrates for High-Quality Thin-Film Fabrication. *Appl. Phys. Lett.* **1995**, *67*, 2615.

(16) Yoshimoto, M.; Sasaki, A.; Akiba, S. Nanoscale Epitaxial Growth Control of Oxide Thin Films by Laser Molecular Beam Epitaxy—towards Oxide Nanoelectronics. *Sci. Technol. Adv. Mater.* **2004**, *5* (4), 527–532. https://doi.org/10.1016/j.stam.2004.02.010.

(17) Gudmundsson, J. T.; Anders, A.; Keudell, A. von. Foundations of Physical Vapor Deposition with Plasma Assistance. *Plasma Sources Sci. Technol.* **2022**, *31* (8), 083001. https://doi.org/10.1088/1361-6595/ac7f53.

(18) Craciun, V.; Singh, R. K.; Perriere, J.; Spear, J.; Craciun, D. Epitaxial ZnO Films Grown on Sapphire (001) by Ultraviolet-Assisted Pulsed Laser Deposition. *J. Electrochem. Soc.* **2000**, *147* (3), 1077. https://doi.org/10.1149/1.1393316.

(19) Nistor, M.; Millon, E.; Cachoncinlle, C.; Seiler, W.; Jedrecy, N.; Hebert, C.; Perrière, J. Transparent Conductive Nd-Doped ZnO Thin Films. *J. Phys. Appl. Phys.* **2015**, *48* (19), 195103. https://doi.org/10.1088/0022-3727/48/19/195103.

(20) Tachiki, M.; Hosomi, T.; Kobayashi, T. Room-Temperature Heteroepitaxial Growth of NiO Thin Films Using Pulsed Laser Deposition. *Jpn. J. Appl. Phys.* **2000**, *39* (4R), 1817. https://doi.org/10.1143/JJAP.39.1817.

(21) Ohnishi, T.; Yoshimoto, M.; Lee, G. H.; Maeda, T.; Koinuma, H. Unit Cell Layer-by-Layer Heteroepitaxy of BaO Thin Films at Temperatures as Low as 20 °C. *J. Vac. Sci. Technol. A* **1997**, *15* (5), 2469–2472. https://doi.org/10.1116/1.580911.

(22) Yoshimoto, M.; Shimozono, K.; Maeda, T.; Ohnishi, T.; Kumagai, M.; Chikyow, T.; Ishiyama, O.; Shinohara, M.; Koinuma, H. K. H. Room-Temperature Epitaxial Growth of CeO2 Thin Films on Si(111) Substrates for Fabrication of Sharp Oxide/Silicon Interface. *Jpn. J. Appl. Phys.* **1995**, *34* (6A), L688. https://doi.org/10.1143/JJAP.34.L688.

(23) Furusawa, M.; Tashiro, J.; Sasaki, A.; Nakajima, K.; Takakura, M.; Chikyow, T.; Ahmet, P.; Yoshimoto, M. In Situ Analysis of the Room-Temperature Epitaxial Growth of CeO2 Ultrathin Films on Si (111) by Coaxial Impact-Collision Ion Scattering Spectroscopy. *Appl. Phys. Lett.* **2001**, *78* (13), 1838–1840. https://doi.org/10.1063/1.1356451.

(24) Ami, T.; Ishida, Y.; Nagasawa, N.; Machida, A.; Suzuki, M. Room-Temperature Epitaxial Growth of CeO2(001) Thin Films on Si(001) Substrates by Electron Beam Evaporation. *Appl. Phys. Lett.* **2001**, *78* (10), 1361–1363. https://doi.org/10.1063/1.1351849.

(25) Tashiro, J.; Sasaki, A.; Akiba, S.; Satoh, S.; Watanabe, T.; Funakubo, H.; Yoshimoto, M. Room-Temperature Epitaxial Growth of Indium Tin Oxide Thin Films on Si Substrates with an Epitaxial CeO2 Ultrathin Buffer. *Thin Solid Films* **2002**, *415* (1), 272–275. https://doi.org/10.1016/S0040-6090(02)00623-5.

(26) Zhu, Z.; Ma, J.; Luan, C.; Mi, W.; Lv, Y. Twin Structures of Epitaxial SnO2 Films Grown on A-Cut Sapphire by Metalorganic Chemical Vapor Deposition. *J. Vac. Sci. Technol. A* **2012**, *30* (2), 021503. https://doi.org/10.1116/1.3683042.

(27) Kim, D. H.; Kwon, J.-H.; Kim, M.; Hong, S.-H. Structural Characteristics of Epitaxial SnO2 Films Deposited on A- and m-Cut Sapphire by ALD. *J. Cryst. Growth* **2011**, *322* (1), 33–37. https://doi.org/10.1016/j.jcrysgro.2011.03.004.

(28) Kurian, J.; Naito, M. Growth of Epitaxial CeO2 Thin Films on R-Cut Sapphire by Molecular Beam Epitaxy. *Phys. C Supercond.* **2004**, *402* (1), 31–37. https://doi.org/10.1016/j.physc.2003.08.007.

(29) Sunder, M.; Moran, P. D. How R-Plane Al2O3 Surface Modifications Impact the Growth of Epitaxial (001) CeO2 Thin Films. *J. Electron. Mater.* **2009**, *38* (9), 1931–1937. https://doi.org/10.1007/s11664-009-0864-6.

(30) Pant, P.; Budai, J. D.; Aggarwal, R.; Narayan, R. J.; Narayan, J. Thin Film Epitaxy and Structure Property Correlations for Non-Polar ZnO Films. *Acta Mater.* **2009**, *57* (15), 4426–4431. https://doi.org/10.1016/j.actamat.2009.05.031.

(31) Han, S. K.; Hong, S. K.; Lee, J. W.; Lee, J. Y.; Song, J. H.; Nam, Y. S.; Chang, S. K.; Minegishi, T.; Yao, T. Structural and Optical Properties of Non-Polar A-Plane ZnO Films Grown on R-Plane Sapphire Substrates by Plasma-Assisted Molecular-Beam Epitaxy. *J. Cryst. Growth* **2007**, *309* (2), 121–127. https://doi.org/10.1016/j.jcrysgro.2007.09.025.

(32) Wang, X.; Aroonyadet, N.; Zhang, Y.; Mecklenburg, M.; Fang, X.; Chen, H.; Goo, E.; Zhou, C. Aligned Epitaxial SnO2 Nanowires on Sapphire: Growth and Device Applications. *Nano Lett.* **2014**, *14* (6), 3014–3022. https://doi.org/10.1021/nl404289z.

(33) Rafique, S.; Han, L.; Zhao, H. Synthesis of Wide Bandgap Ga2O3 (Eg ~ 4.6–4.7 EV) Thin Films on Sapphire by Low Pressure Chemical Vapor Deposition. *Phys. Status Solidi A* **2016**, *213* (4), 1002–1009. https://doi.org/10.1002/pssa.201532711.

(34) Yamashita, Y.; Honda, K.; Yagi, T.; Jia, J.; Taketoshi, N.; Shigesato, Y. Thermal Conductivity of Hetero-Epitaxial ZnO Thin Films on c- and r-Plane Sapphire Substrates: Thickness and Grain Size Effect. *J. Appl. Phys.* **2019**, *125* (3), 035101. https://doi.org/10.1063/1.5055266.

(35) Perrière, J.; Hebert C.; Nistor M.; Millon E.; Ganem J.J.; Jedrecy N. $Zn_{1-x}Fe_xO$ films: from transparent Fe-diluted ZnO wurtzite to magnetic Zn diluted Fe_3O_4 spinel. *J. Mat. Chem.* **2015***, 3,* 11239-11249.

https://doi.org/10.1039/C5TC02090E

(36) Sano, T.; Tsuji, M.; Tamaura, Y. Effect of Foreign cations of Zn (II) or Mn (II) ion in FeO-wustite on its disproportionation reaction below 575˚C. *Solid State Ionics* **1997***, 104,* 311-317.

https://doi.org/10.1016/S0167-2738(97)00432-3

(37) Versluijs, J. J.; Bari, M. A.; Coey, J. M. D. Magnetoresistance of Half-Metallic Oxide Nanocontacts. *Phys. Rev. Lett.* **2001**, *87* (2), 026601. https://doi.org/10.1103/PhysRevLett.87.026601.

(38) Hu, G.; Suzuki, Y. Negative Spin Polarization of Fe3O4 in Magnetite/Manganite-Based Junctions. *Phys. Rev. Lett.* **2002**, *89* (27), 276601. https://doi.org/10.1103/PhysRevLett.89.276601.

(39) Seki, M.; Takahashi, M.; Adachi, M.; Yamahara, H.; Tabata, H. Fabrication and Characterization of Wüstite-Based Epitaxial Thin Films: P-Type Wide-Gap Oxide

Semiconductors Composed of Abundant Elements. *Appl. Phys. Lett.* **2014**, *105* (11), 112105. https://doi.org/10.1063/1.4896316.

(40) Fuji, Y.; Hara, M.; Yuasa, H.; Murakami, S.; Fukuzawa, H. Enhancement of Magnetoresistance by Ultra-Thin Zn Wüstite Layer. *Appl. Phys. Lett.* **2011**, *99* (13), 132103. https://doi.org/10.1063/1.3644470.

(41) Narayan, J.; Dovidenko, K.; Sharma, A. K.; Oktyabrsky, S. Defects and Interfaces in Epitaxial ZnO/α-Al2O3 and AlN/ZnO/α-Al2O3 Heterostructures. *J. Appl. Phys.* **1998**, *84* (5), 2597–2601. https://doi.org/10.1063/1.368440.

(42) Narayan, J.; Pant, P.; Chugh, A.; Choi, H.; Fan, J. C. C. Characteristics of Nucleation Layer and Epitaxy in GaN/Sapphire Heterostructures. *J. Appl. Phys.* **2006**, *99* (5), 054313. https://doi.org/10.1063/1.2178660.

(43) Seiler, W.; Nistor, M.; Hebert, C.; Perrière, J. Epitaxial Undoped Indium Oxide Thin Films: Structural and Physical Properties. *Sol. Energy Mater. Sol. Cells* **2013**, *116*, 34–42. https://doi.org/10.1016/j.solmat.2013.04.002.

(44) Sbaï, N.; Perrière, J.; Seiler, W.; Millon, E. Epitaxial Growth of Titanium Oxide Thin Films on C-Cut and α-Cut Sapphire Substrates. *Surf. Sci.* **2007**, *601* (23), 5649–5658. https://doi.org/10.1016/j.susc.2007.09.019.

(45) Hoghooghi, B.; Raj, R. Controlled Epitaxial Nucleation of Nickel Oxide on Microfabricated Magnesium Oxide Substrates in a CVD Process. *J. Am. Ceram. Soc.* **1996**, *79* (4), 1025–1033. https://doi.org/10.1111/j.1151-2916.1996.tb08543.x.

(46) Mozhaev, P. B.; Mozhaeva, J. E.; Khoryushin, A. V.; Bindslev Hansen, J.; Jacobsen, C. S.; Bdikin, I. K.; Kotelyanskii, I. M.; Luzanov, V. A. Three-Dimensional Graphoepitaxial Growth of

Oxide Films by Pulsed Laser Deposition. *Phys. Rev. Mater.* **2018**, *2* (10), 103401. https://doi.org/10.1103/PhysRevMaterials.2.103401.

(47) Noguera, C. Polar Oxide Surfaces. *J. Phys. Condens. Matter* **2000**, *12* (31), R367. https://doi.org/10.1088/0953-8984/12/31/201.

(48) Chu, Y.-H. Van Der Waals Oxide Heteroepitaxy. *Npj Quantum Mater.* **2017**, *2* (1), 67. https://doi.org/10.1038/s41535-017-0069-9.

(49) Utama, M. I. B.; Zhang, Q.; Jia, S.; Li, D.; Wang, J.; Xiong, Q. Epitaxial II–VI Tripod Nanocrystals: A Generalization of van Der Waals Epitaxy for Nonplanar Polytypic Nanoarchitectures. *ACS Nano* **2012**, *6* (3), 2281–2288. https://doi.org/10.1021/nn204344z.

(50) Ke, S.; Xie, J.; Chen, C.; Lin, P.; Zeng, X.; Shu, L.; Fei, L.; Wang, Y.; Ye, M.; Wang, D. Van Der Waals Epitaxy of Al-Doped ZnO Film on Mica as a Flexible Transparent Heater with Ultrafast Thermal Response. *Appl. Phys. Lett.* **2018**, *112* (3), 031905. https://doi.org/10.1063/1.5010358.

(51) Maréchal, C.; Lacaze, E.; Seiler, W.; Perrière, J. Growth Mechanisms of Laser Deposited BiSrCaCuO Films on MgO Substrates. *Phys. C Supercond.* **1998**, *294* (1–2), 23–32. https://doi.org/10.1016/S0921-4534(97)01735-8.

(52) Portier, X.; Hebert, C.; Briand, E.; Perrière, J.; Millon, E.; Cachoncinlle, C.; Nistor, M.; Jedrecy, N. Microstructure of Nanocomposite Wurtzite-Spinel (Fe:ZnO)-(Zn:Fe3O4) Epitaxial Films. *Mater. Chem. Phys.* **2019**, *229*, 130–138. https://doi.org/10.1016/j.matchemphys.2019.02.089.

(53) Hebert, C. ZnxFe1-XO1+δ Nanocomposite Films: Wurtzite and Spinel Phases, Sorbonne University, Paris, 2017.

(54) Le Boulbar, E.; Millon, E.; Mathias, J.; Boulmer-Leborgne, C.; Nistor, M.; Gherendi, F.; Sbaï, N.; Quoirin, J. B. Pure and Nb-Doped TiO1.5 Films Grown by Pulsed-Laser Deposition for Transparent p–n Homojunctions. *E-MRS 2010 Spring Meet. Symp. R Laser Process. Diagn. Micro Nano Appl.* **2011**, *257* (12), 5380–5383. https://doi.org/10.1016/j.apsusc.2010.10.149.

(55) Chaoui, N.; Millon, E.; Muller, J. F.; Ecker, P.; Bieck, W.; Migeon, H. N. On the Role of Ambient Oxygen in the Formation of Lead Titanate Pulsed Laser Deposition Thin Films. *Appl. Surf. Sci.* **1999**, *138–139*, 256–260. https://doi.org/10.1016/S0169-4332(98)00403-6.

(56) Chaoui, N.; Millon, E.; Muller, J. F.; Ecker, P.; Bieck, W.; Migeon, H. N. Perovskite Lead Titanate PLD Thin Films: Study of Oxygen Incorporation by 18O Tracing Technique. *Mater. Chem. Phys.* **1999**, *59* (2), 114–119. https://doi.org/10.1016/S0254-0584(99)00051-6.

(57) Nistor, M.; Petitmangin, A.; Hebert, C.; Seiler, W. Nanocomposite Oxide Thin Films Grown by Pulsed Energy Beam Deposition. *E-MRS 2010 Spring Meet. Symp. R Laser Process. Diagn. Micro Nano Appl.* **2011**, *257* (12), 5337–5340. https://doi.org/10.1016/j.apsusc.2010.11.139.

(58) Clatot, J.; Nistor, M.; Rougier, A. Influence of Si Concentration on Electrical and Optical Properties of Room Temperature ZnO:Si Thin Films. *Thin Solid Films* **2013**, *531*, 197–202. https://doi.org/10.1016/j.tsf.2013.01.046.

(59) Rodriguez-Carvajal, J. Recent Developments of the Program Fullprof. *Commission on Powder Diffraction (IUCr). Newsletter*. 2001st ed. pp 12–19.

(60) Calvert, C. C.; Brown, A.; Brydson, R. Determination of the Local Chemistry of Iron in Inorganic and Organic Materials. *Electron Energy Loss Spectrosc. Electron Microsc.* **2005**, *143* (2), 173–187. https://doi.org/10.1016/j.elspec.2004.03.012.

(61) Chen, J.; Deng, H.; Ji, H.; Tian, Y. Effect of Substrate Microstructure on the Misorientation of A-Plane ZnO Film Investigated Using x-Ray Diffraction. *J. Vac. Sci. Technol. A* **2011**, *29* (3), 03A116. https://doi.org/10.1116/1.3573670.

(62) Savvides, N.; Thorley, A.; Gnanarajan, S.; Katsaros, A. Epitaxial Growth of Cerium Oxide Thin Film Buffer Layers Deposited by d.c. Magnetron Sputtering. *Thin Solid Films* **2001**, *388* (1), 177–182. https://doi.org/10.1016/S0040-6090(01)00839-2.

(63) Wang, F.; Müller, S.; Wördenweber, R. Large-Area Epitaxial MgO Buffer Layers on Sapphire Substrates for Y-Ba-Cu-O Dilm Deposition. *Thin Solid Films* **1993**, *232* (2), 232–236. https://doi.org/10.1016/0040-6090(93)90014-G.

(64) P A Stampe; M Bullock; W P Tucker; Robin J Kennedy. Growth of MgO Thin Films on M-, A-, C- and R-Plane Sapphire by Laser Ablation. *J. Phys. Appl. Phys.* **1999**, *32* (15), 1778. https://doi.org/10.1088/0022-3727/32/15/304.

(65) Malikov, I. V.; Berezin, V. A.; Fomin, L. A.; Chernykh, A. V. Epitaxial Fe3O4 Films Grown on R-Plane Sapphire by Pulsed Laser Deposition. *Inorg. Mater.* **2020**, *56* (2), 164–171. https://doi.org/10.1134/S0020168520020120.

(66) Zheleva, T.; Jagannadham, K.; Narayan, J. Epitaxial-Growth in Large-Lattice-Mismatch Systems. *J. Appl. Phys.* **1994**, *75* (2), 860–871. https://doi.org/10.1063/1.356440.

(67) Bick, D. S.; Sharath, S. U.; Hoffman, I.; Major, M.; Kurian, J.; Alff, L. (001) and (111) Single-Oriented Highly Epitaxial CeO2 Thin Films on r-Cut Sapphire Substrates. *J. Electron. Mater.* **2015**, *44* (8), 2930–2938. https://doi.org/10.1007/s11664-015-3728-2.

(68) Zhao, P.; Ito, A.; Tu, R.; Goto, T. High-Speed Epitaxial Growth of (100)-Oriented CeO2 Film on r-Cut Sapphire by Laser Chemical Vapor Deposition. *Surf. Coat. Technol.* **2011**, *205* (16), 4079–4082. https://doi.org/10.1016/j.surfcoat.2011.02.062.

(69) Yamamoto, S.; Sugimoto, M.; Koshikawa, H.; Hakoda, T.; Yamaki, T. Orientational Control of CeO2 Films on Sapphire Substrates Grown by Magnetron Sputtering. *18th Int. Conf. Cryst. Growth Epitaxy ICCGE-18* **2017**, *468*, 262–267. https://doi.org/10.1016/j.jcrysgro.2016.12.038.

"For Table of Contents Use Only"

Room temperature epitaxial growth of Zn-doped iron oxide films on c-, a- and r-cut sapphire substrates

Valérie Demange, Xavier Portier, Sophie Ollivier, Mathieu Pasturel, Thierry Roisnel, Maryline Guilloux-Viry, Christian Hebert, Magdalena Nistor, Christophe Cachoncinlle, Eric Millon, Jacques Perrière

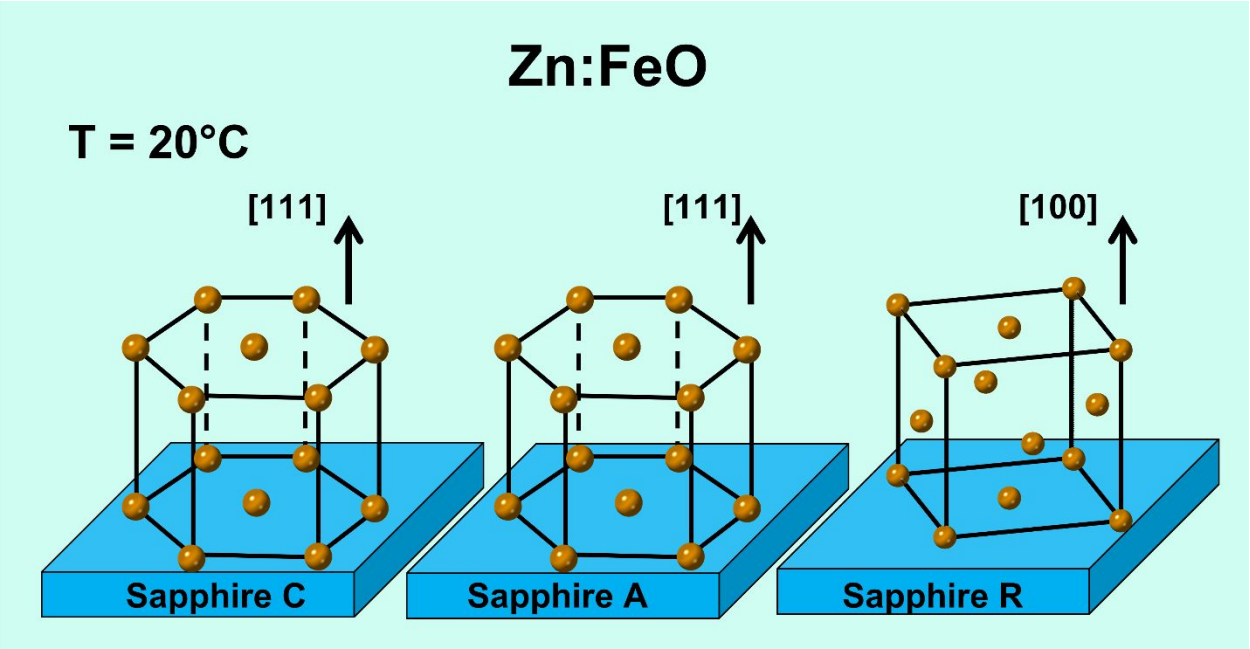

Synopsis: Room-temperature epitaxial growth of Zn doped FeO wüstite thin films on c-cut, a-cut and r-cut sapphire substrates

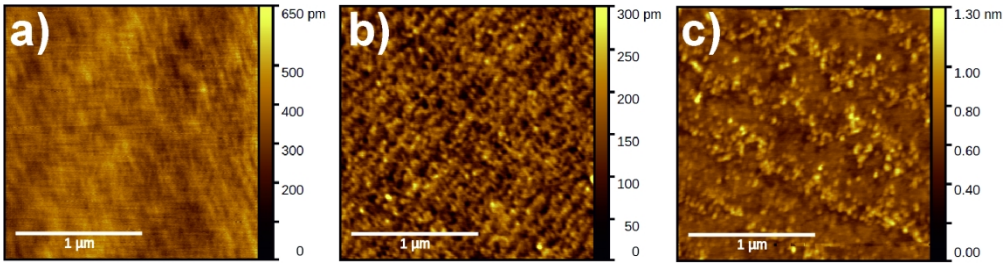

Figure 1. AFM image of c-cut, a-cut and r-cut sapphire substrates without any annealing before the PLD growth.

181x47mm (300 x 300 DPI)

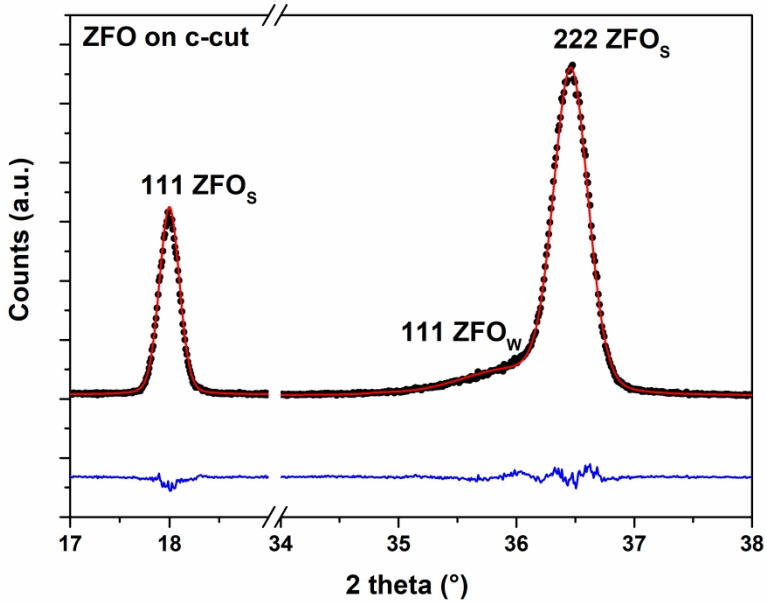

Figure 2. Experimental θ-2θ XRD pattern (black symbols) of the ZFO film grown on c-cut sapphire substrate showing a peak at about 18° corresponding to the 111 Bragg reflection of the spinel phase and a broad peak around 36° corresponding to the 111 reflection of wüstite and the 222 reflection of spinel phases, respectively. This pattern has been refined using the Le Bail method and calculated and difference patterns are shown as red and blue lines, respectively.

288x201mm (300 x 300 DPI)

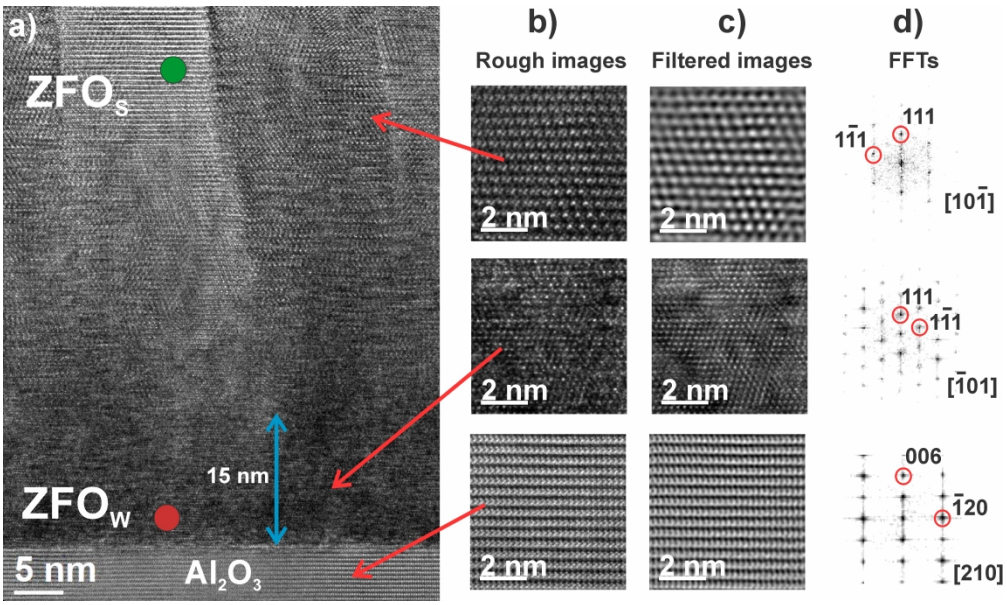

Figure 3. a) HREM image of a cross section of a ZFO film on c-cut sapphire substrate showing a thin region of ZFOW at the bottom of the film; b) and c) are enlarged regions of the different parts of the film and the Al2O3 sapphire substrate corresponding to rough and filtered images respectively; d) FFTs of the previous mentioned images leading to the identification of the structures.

385x229mm (300 x 300 DPI)

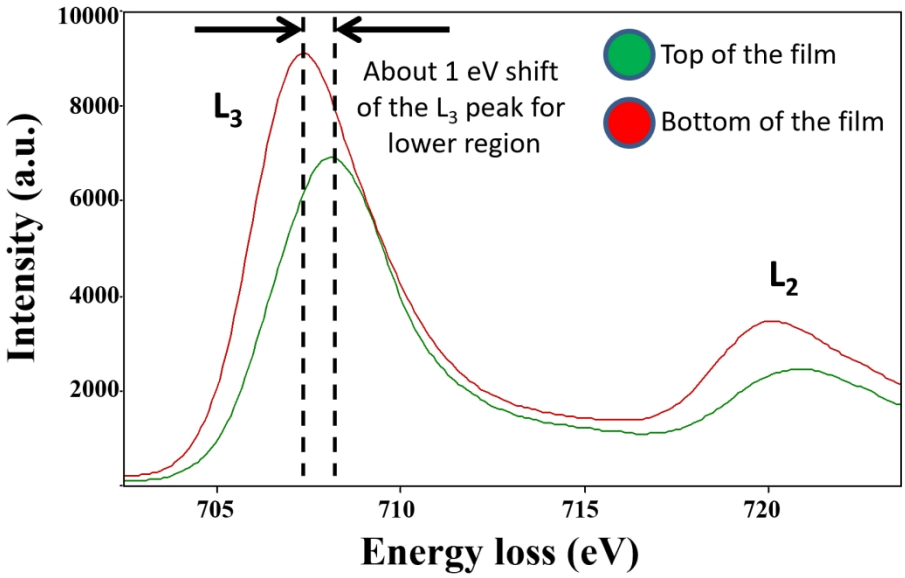

Figure 4. EELS spectra of the L3 and L2 energy thresholds of Fe. A 1 eV shift of the L3 peak confirms the lowering of the valence state of Fe and thus the presence of wüstite at the bottom of the film.

141x90mm (330 x 330 DPI)

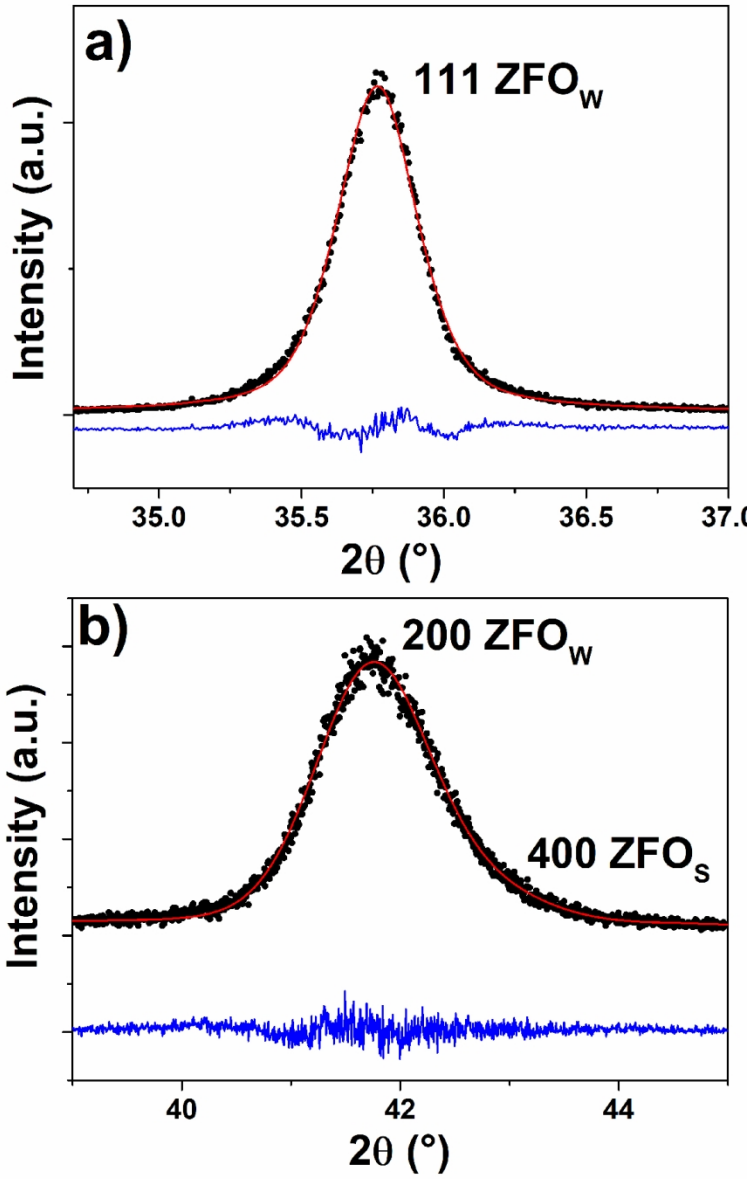

Figure 5. Le Bail refined θ-2θ XRD patterns of ZFO films grown on a-cut (a) and r-cut (b) sapphire substrates. Black symbols display the experimental data, red lines represent the theoretical patterns and blue curves show the difference between them.

102x161mm (300 x 300 DPI)

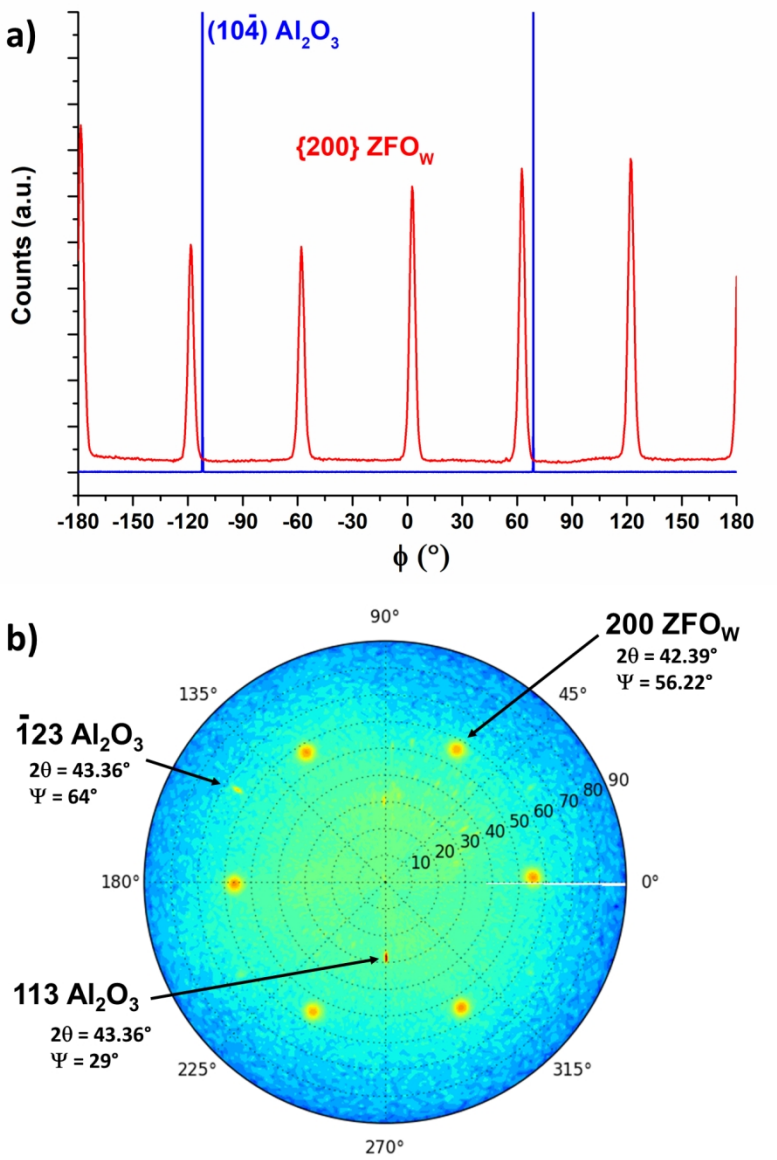

Figure 6. a) Phi-scan of the {200} planes of the (111) ZFOw film (red) and of the (10-4) planes of the a-cut sapphire substrate (blue). b) Pole figure of the {200} planes of the (111) ZFOw film showing 6 poles.

230x346mm (150 x 150 DPI)

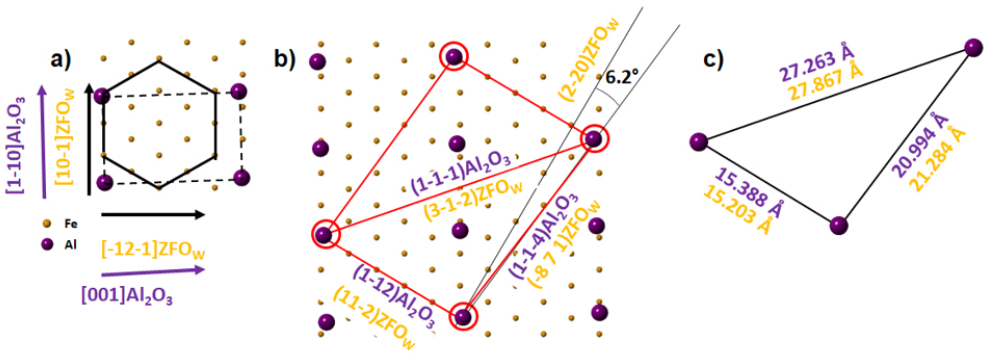

Figure 7: a) Scheme of the epitaxy of (111) ZFO_W grown on the a-cut sapphire substrate, determined by phi-scans measurement. b) Scheme of the domain matching epitaxy of (111) ZFO_W grown on the a-cut sapphire substrate, showing the site coincidences between the two lattices. The 6.2° rotation between the (2-20) ZFO_W plane and the (1-1-4) sapphire plane highlighted in the phi-scans is shown. c) Interatomic distances of the two lattices reported on the scheme.

254x93mm (96 x 96 DPI)

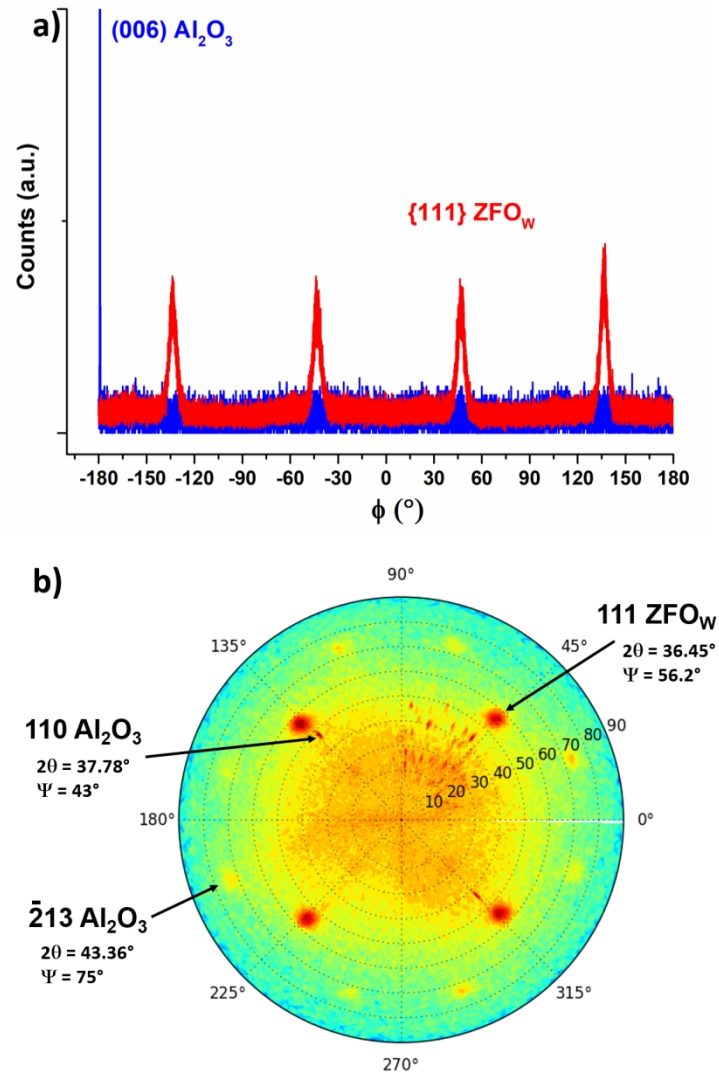

Figure 8: a) Phi-scan of the {111} planes of the (100) ZFOw film (red) and of the (006) plane of the r-cut sapphire substrate (blue). b) Pole figure of the {111} planes of the (100) ZFOw film showing 4 poles.

251x376mm (150 x 150 DPI)

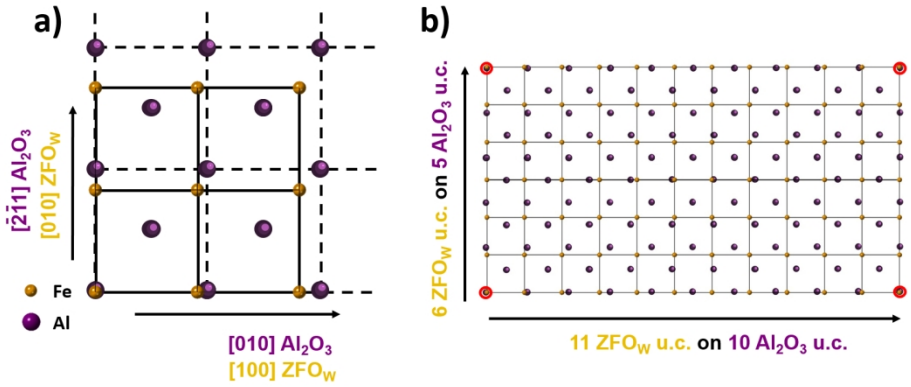

Figure 9: a) Scheme of the epitaxy of (100) ZFOw grown on r-cut sapphire substrate. b) Scheme of domain matching epitaxy of (100) ZFOw grown on r-cut sapphire substrate.

309x138mm (150 x 150 DPI)